Supplement of Geosci. Model Dev., 18, 6415–6438, 2025
https://doi.org/10.5194/gmd-18-6415-2025-supplement
© Author(s) 2025. CC BY 4.0 License.

Geoscientific Model Development
Open Access
EGU

Supplement of

BIOPERIANT12: a mesoscale-resolving coupled physics–biogeochemical model for the Southern Ocean

Nicolette Chang et al.

Correspondence to: Nicolette Chang (nchang@csir.co.za)

The copyright of individual parts of the supplement might differ from the article licence.

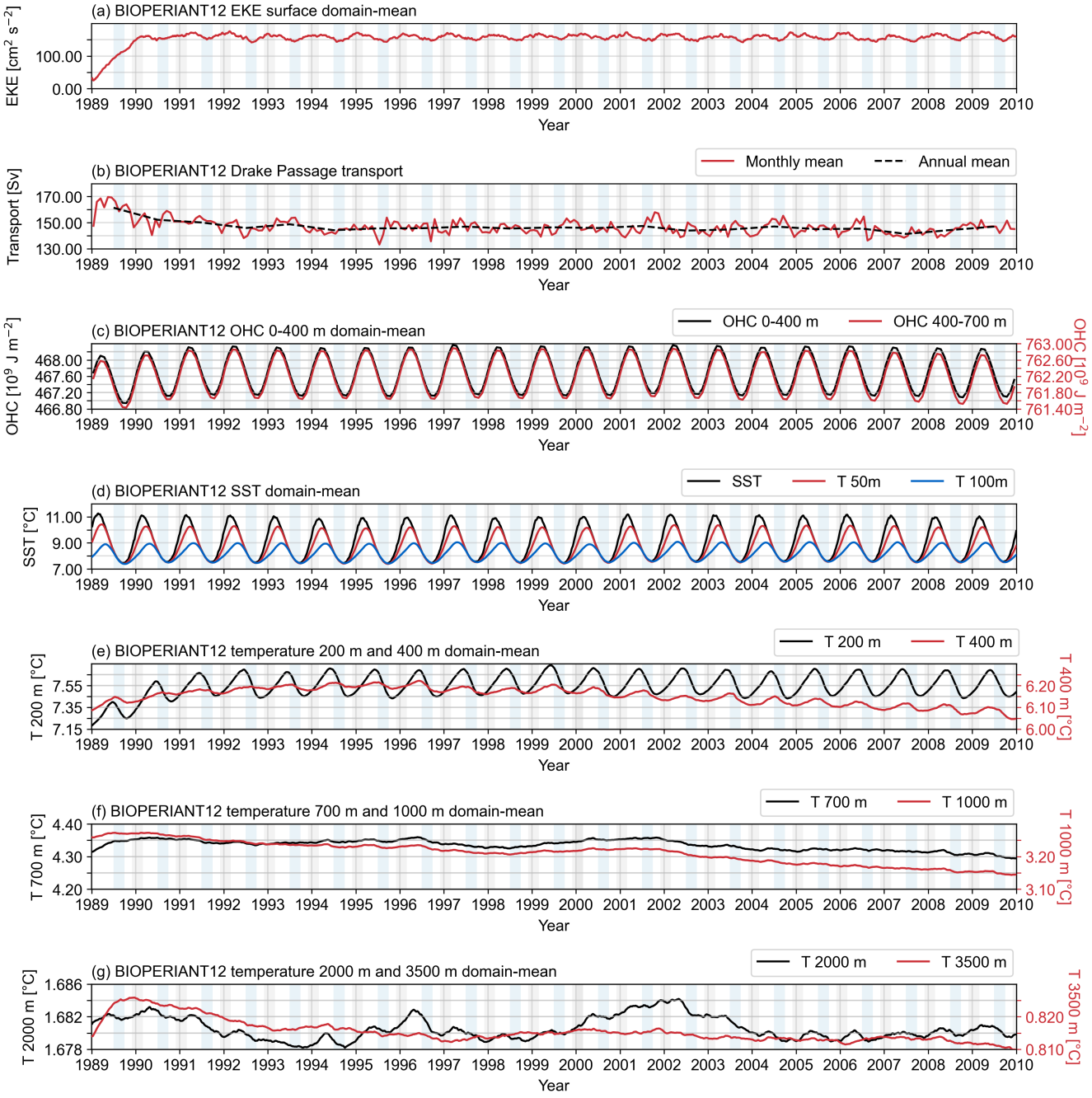

Figure S1. Evolution of the BIOPERIANT12 configuration **(a)** 5–day mean, domain-averaged, surface EKE ($cm^2 s^{-2}$); **(b)** zonal transport (Sv) through the Drake Passage, monthly and annual means shown; **(c)** domain-mean ocean heat content (OHC) for 0–400 m and 400-700 m. Evolution of domain-mean model temperature at (d) surface, 5 m and 100 m; (e) 200 m, 400 m, (f) 700 m, 1000 m, and (g) 2000 m and 3000 m.

S2 Expansion on BIOPERIANT12 ocean dynamic metrics

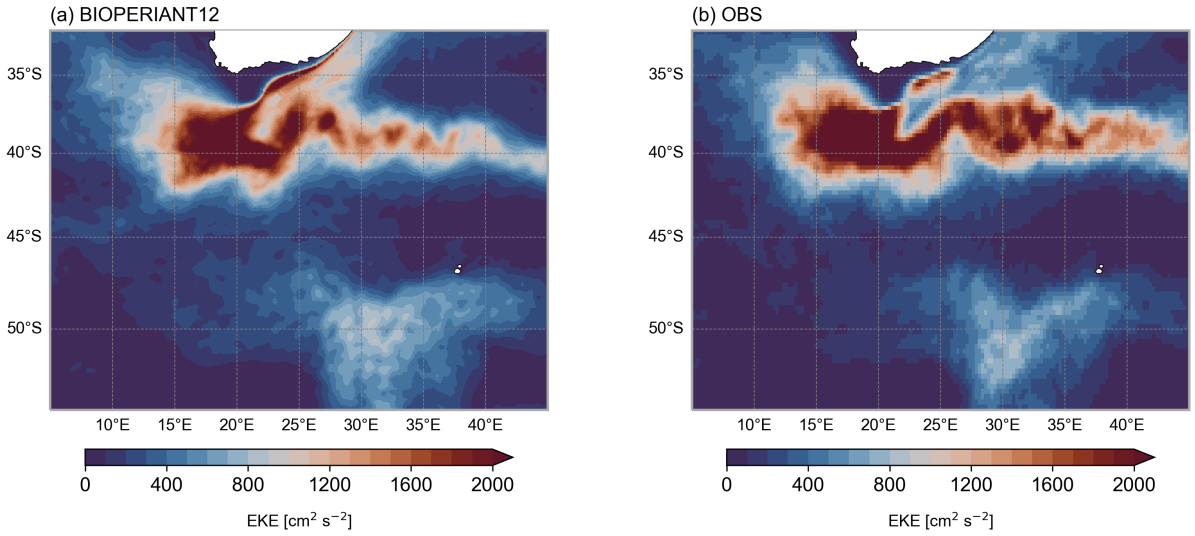

Figure S2. EKE 2000–2009 annual mean as in Fig. 2, subset for the Agulhas Current retroflection region for **(a)** BIOPERIANT12 output and **(b)** AVISO data .

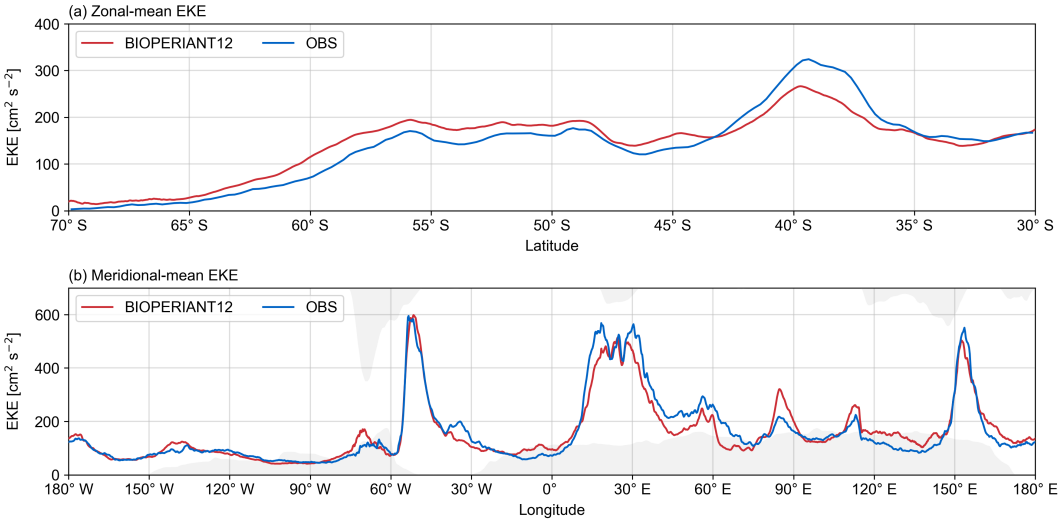

Figure S3. BIOPERIANT12 versus AVISO-derived EKE 2000–2009 annual mean spatially averaged **(a)** zonally, **(b)** meridionally.

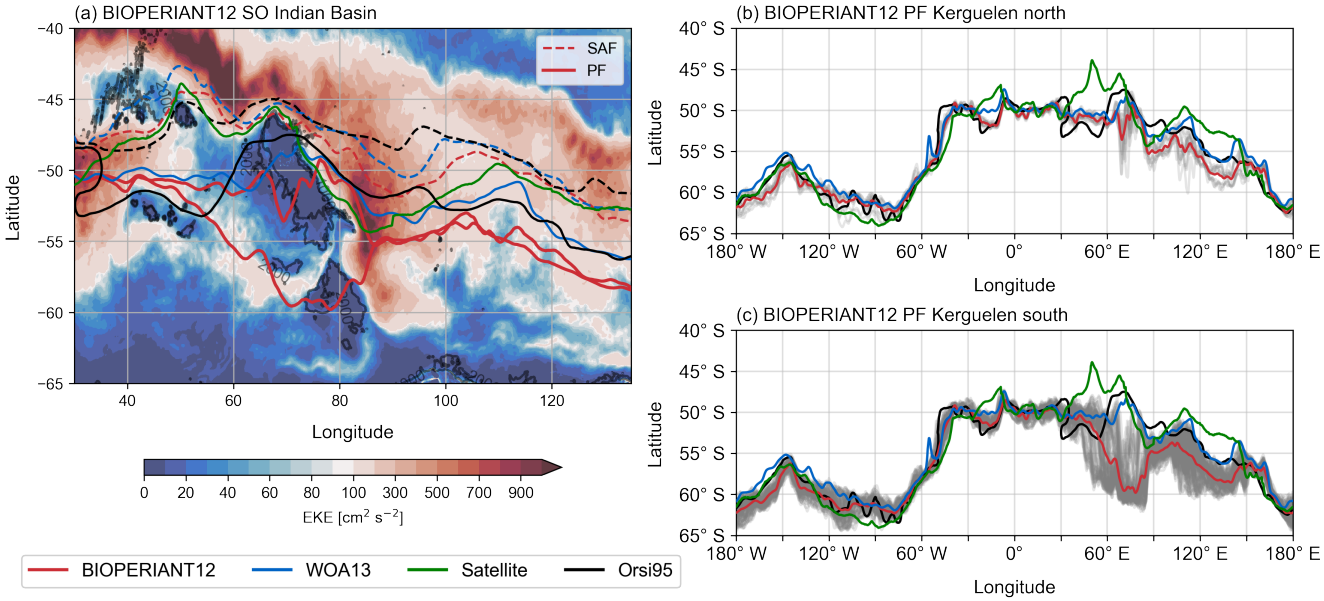

Figure S4. SubAntarctic Front (SAF) and Antarctic Polar Front (PF) locations at the Kerguelen Plateau for BIOPERIANT12, WOA13-derived, and from (Orsi et al., 1995) and satellite PF locations from (Freeman and Lovenduski, 2016) overlying model climatological-mean EK **(a)** . Comparison of monthly-mean model PF locations (grey lines) for an average **(b)** northward path versus **(c)** southward path at 70-80°S, against the annual mean fronts as shown in left panel and in Fig. 4. The red line is the mean latitude of the grey lines, i.e. the model-mean latitude of the north and south paths.

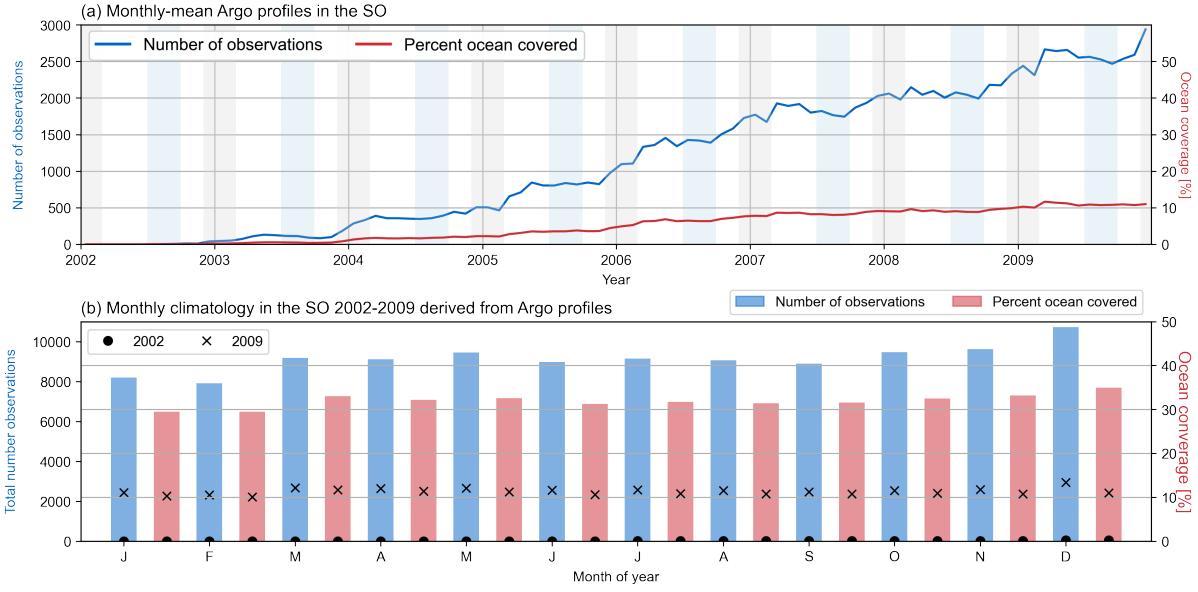

Figure S5. Argo profiles and their weakness determining MLD depths for the decade 2000–2009 **(a)** Increasing numbers of observations available for the Southern Ocean through time for model analysis period, and the coverage as a percentage of the total Southern Ocean as represented by a 1°x 1°grid. **(b)** Bar chart of ARGO profile observations available per month for Southern Ocean between 70°S and 30°S for the period 2002–2009, with number of observations for year 2002 and year 2009 marked for comparison.

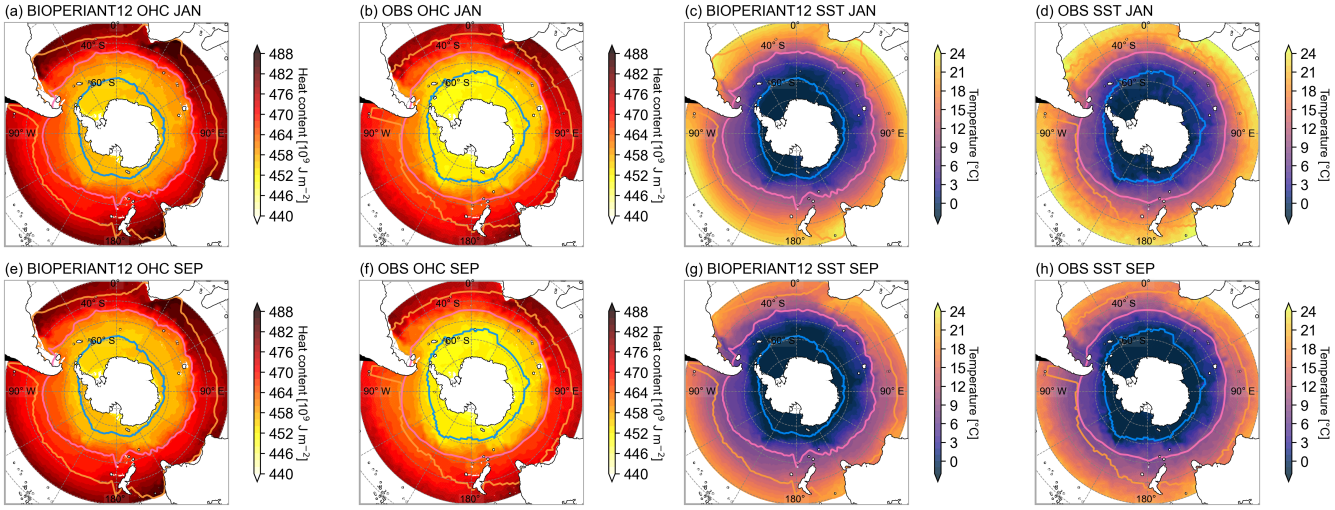

Figure S6. Seasonal climatological maps for ocean heat content (OHC, a,b,e,f) and for sea surface temperature (SST, c,d,g.h) for BIOPERIANT12 and WOA13 showing large-scale similarities.

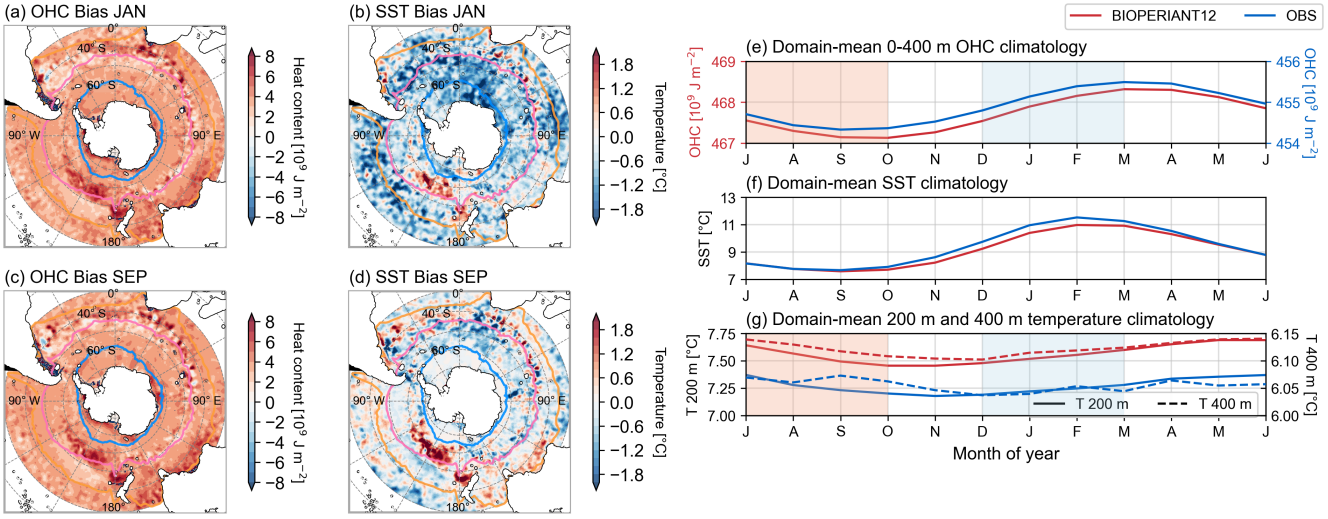

Figure S7. Climatological mean bias (BIOPERIANT12 - WOA13 dataset) for ocean heat content in the upper 400 m in **(a)** January and **(c)** September, and for SST in **(b)** January and **(d)** September. Climatological seasonal cycle (2000–2009) for BIOPERIANT12 versus WOA13 of (e) upper 400 m ocean heat content (note each source has its own y axis for clarity), (f) SST, (g) temnperature at 200 m and at 400 m.

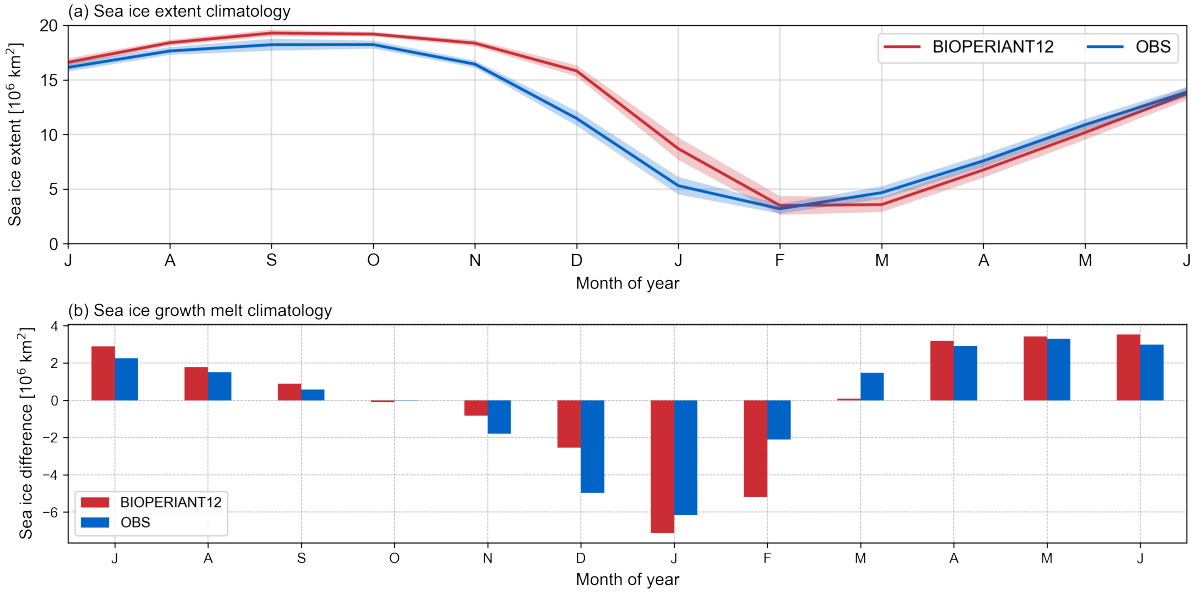

Figure S8. (a) Climatological seasonal cycle of sea-ice in BIOPERIANT12 versus NSIDC sea ice data, showing that the model minimum sea ice extent is similar in February and March. **(b)** Alternative view of sea ice melt and growth in BIOPERIANT12, as presented in manuscript Fig. 5.

S3 BIOPERIANT12 biome definition and characterisation

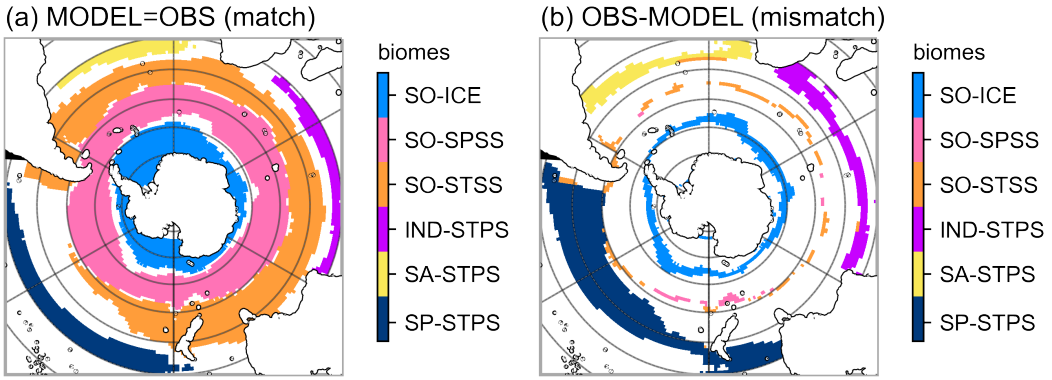

Figure S9. Comparison of biome definition in BIOPERIANT12 compared to the observation-derived mean biome from Fay and McKinley (2014) (south of 30°S) showing **(a)** regions the biome locations for both sources agree, white showing model regions with unassigned biomes, and **(b)** the observational biomes corresponding to the unassigned model regions.

To quantify the percentage of overlap between the observation-based and modelled mean biomes (Fig. 6), we first regridded the biomes from BIOPERIANT12 onto the regular 1°x 1°grid. From there, we identify that there is a 97 % spatial agreement between the observed and modelled SO-SPSS biomes, followed by SO-ICE and SO-STPS with 71 % and 63 % of spatial agreement, respectively. The subtropical biomes however present an averaged spatial agreement of 34 %, which is mostly due to the "biome-free" zones in the model, the white unassigned regions in the mean biome in Fig. 9a). In Fig. 9b, the white zones are assigned to the biome from the datasets to examine the the individual characteristics of the subtropical regions in BIOPERIANT12 that were not assigned to any biomes. For the STPS of the southern Pacific, Atlantic and Indian basins (Fig. 10a–f), we find that the biome-free zones could neither be assigned to the STPS biome nor to the STSS biome, as the summer Chl-a exceeds the STPS biome's upper limit of 0.25 mg m^{-3}, particularly downstream of continents or in region of potential high eddy kinetic energy(Fig. 10b, e) but while satisfying the Chl-a criteria for the STSS (Fig. 10h), did not meet the STSS maximum MLD criteria of greater than 150 m (Fig. 10c, f, i).

The unmatched criteria explain an absence of biome definitions in the subtropical areas of BIOPERIANT12. Nevertheless, it is worth pointing out that Fay and McKinley (2014) developed their biome criteria using a relatively low resolution approach (1°x 1°), which may not reflect some of the high eddy kinetic energy regions, such as the subtropical branch of Southern Ocean. The biome-free zones in BIOPERIANT12 might therefore be explained by the fact that the model's high resolution (1/12°) potentially captures a new biome category.

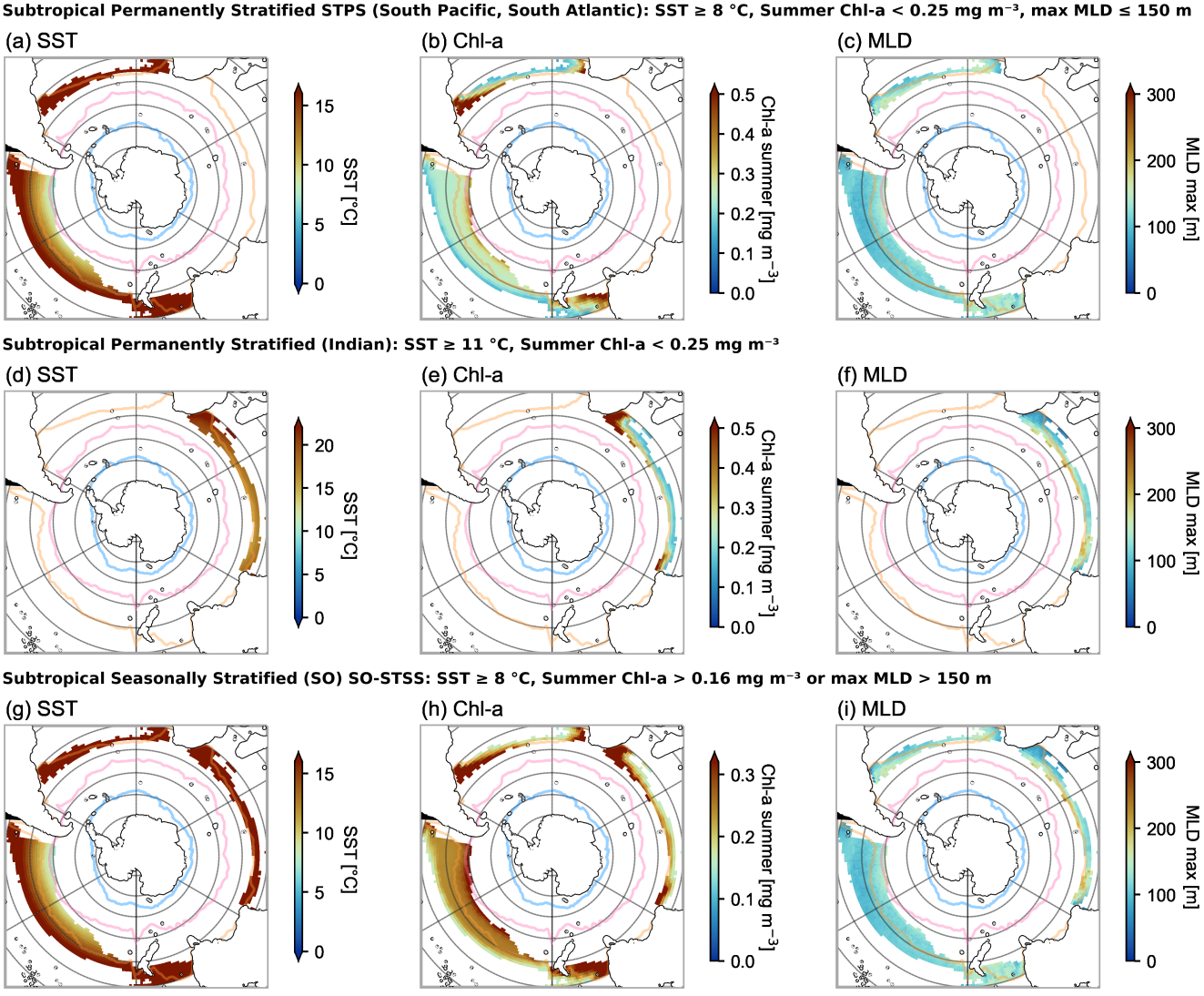

Figure S10. BIOPERIANT12 SST, chlorophyll and MLD showing incompatibility with biome-definition criteria for the STPS and STSS biomes (Fay and McKinley, 2014).

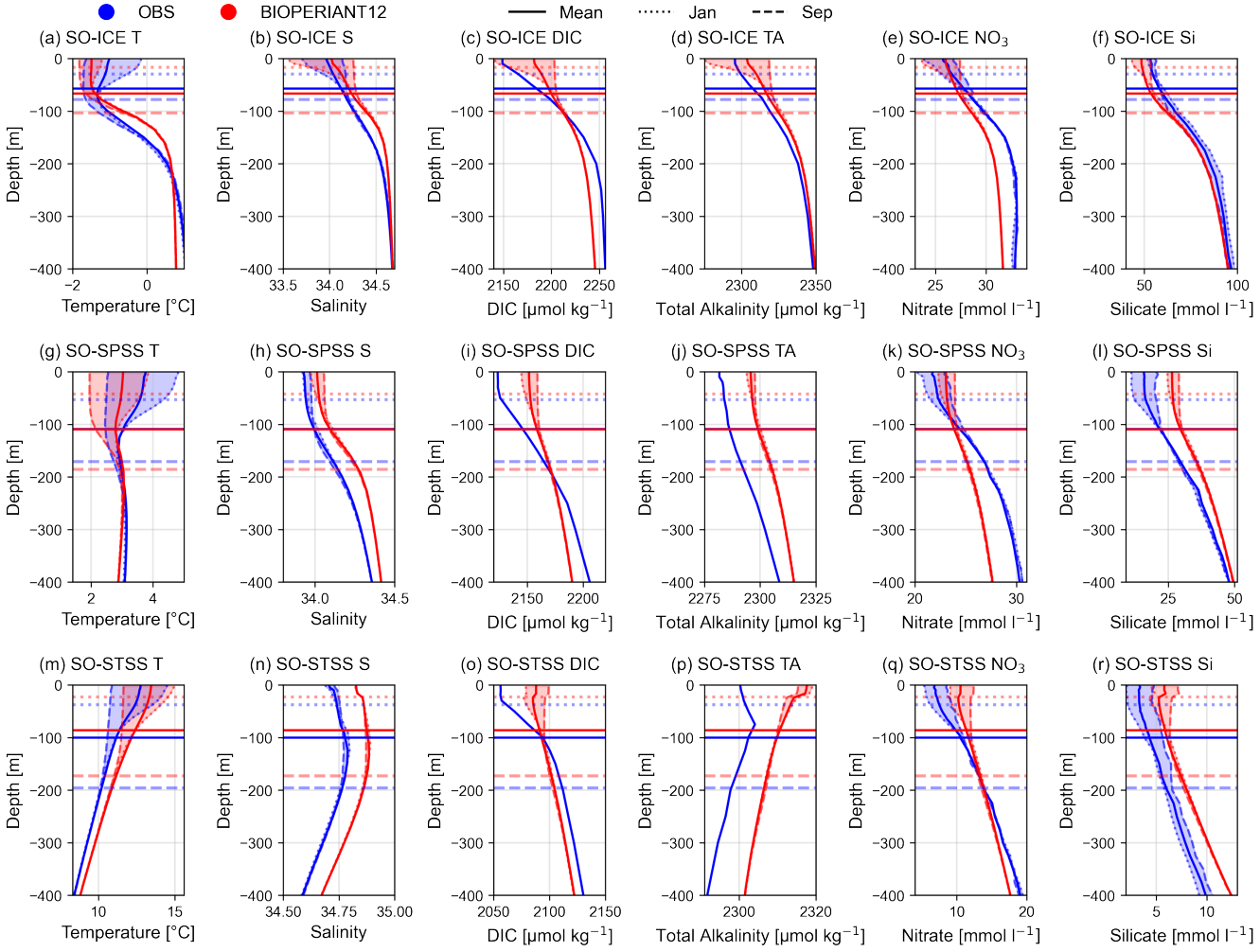

Figure S11. Observation vs model biome-mean profiles (2000–2009) for selected variables showing annual (solid line), January (dotted line), and September (dashed line) climatological means with MLD overlaid.

Table S1. Seasonal cycle 200 m climatology per biome: BIOPERIANT12 (BP12) vs observations (OBS): area-weighted Mean and Amplitude (difference between maximum and minimum) for the respective data sources; Seasonality/SCR (the correlation of the interannual varying timeseries against its climatological seasonal cycle) for the model only; and for comparison Correlation (correlation coefficient), RSD (ratio of BP12:OBS standard deviation), Model Reliability Index (log-transform error).

Variable								Variable							
	Biome	SO-ICE		SO-SPSS		SO-STSS			Biome	SO-ICE		SO-SPSS		SO-STSS	
		BP12	OBS	BP12	OBS	BP12	OBS			BP12	OBS	BP12	OBS	BP12	OBS
Temperature	Mean	0.63	0.54	3.05	3.02	10.94	10.17	Salinity	Mean	34.61	34.55	34.28	34.17	34.87	34.76
[°C]	Amplitude	0.04	0.21	0.30	0.34	0.35	0.33	[]	Amplitude	0.01	0.03	0.02	0.04	0.02	0.04
	Correlation		**0.35**		0.99		0.98		Correlation		**-0.68**		0.97		0.96
	RSD	**0.18**		0.89		1.08			RSD	**0.38**		0.52		0.55	
	Model RI	1.22		1.01		1.08			Model RI	1.00		1.00		1.00	
DIC	Mean	2233.28	2246.63	2171.79	2173.44	2103.85	2112.02	Tot. Alkalinity	Mean	2339.70	2337.97	2305.78	2293.88	2306.65	2297.78
$[\mu molkg^{-1}]$	Amplitude	0.42	0.00	2.19	0.00	3.02	0.00	$[\mu molkg^{-1}]$	Amplitude	0.60	0.00	1.42	0.00	0.85	0.00
	Model RI	1.01		1.00		1.00			Model RI	1.00		1.01		1.00	
Nitrate	Mean	30.78	32.64	25.50	27.42	13.75	13.90	Phosphate	Mean	2.14	2.27	1.78	1.90	0.99	1.03
$[mmoll^{-1}]$	Amplitude	0.04	0.83	0.32	0.95	0.62	0.65	$[mmoll^{-1}]$	Amplitude	0.00	0.06	0.02	0.10	0.04	0.07
	Correlation		**0.26**		**0.07**		**0.47**		Correlation		**0.34**		**-0.08**		**-0.64**
	RSD	**0.06**		**0.41**		1.08			RSD	**0.09**		**0.25**		0.65	
	Model RI	1.06		1.08		1.02			Model RI	1.06		1.07		1.05	
Silicate	Mean	81.70	85.41	37.57	33.06	7.84	6.08	Diss. O_2	Mean	248.21	231.83	291.67	279.58	260.27	257.76
$[mmoll^{-1}]$	Amplitude	0.42	6.20	1.23	3.56	0.47	1.02	$[\mu moll^{-1}]$	Amplitude	1.37	18.45	11.35	19.19	8.36	12.57
	Correlation		0.73		**0.18**		**-0.75**		Correlation		**0.20**		0.94		0.98
	RSD	**0.08**		**0.47**		**0.48**			RSD	**0.10**		0.73		0.74	
	Model RI	1.05		1.14		1.30			Model RI	1.07		1.04		1.01	

[a] GLODAPv2 observations are an annual mean product.
RSD:SD of BP12 greater (less) than that of OBS by factor 1.5 (0.5). **Correlation**: BP12-OBS correlation coefficient less than 0.5.
SCR: BP12 greater than 0.65 (medium to high). **Model RI**: greater 1.5 (medium to high).

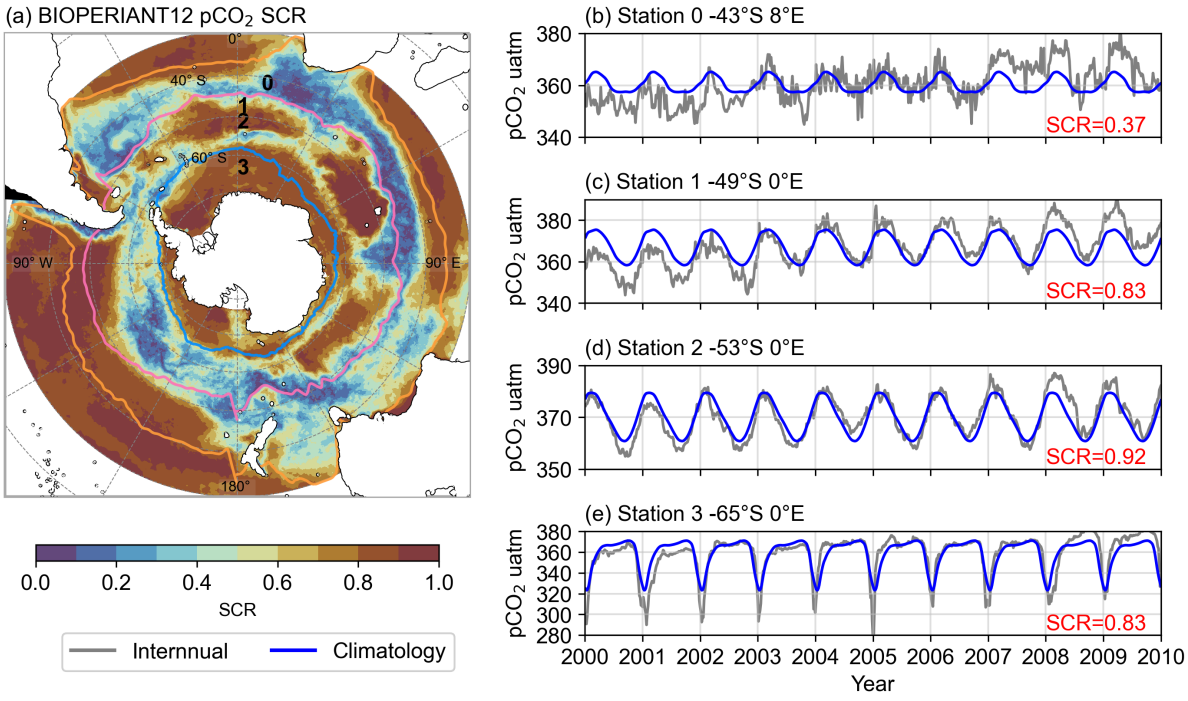

Figure S12. (a) BIOPERIANT12 pCO_2 seasonal cycle reproducibility with northern biome boundaries overlaid and **(b-d)** pCO_2 interannual model time series against its repeated climatological timeseries at selected grid cells (0–3 displayed on map and described in axis title), comparing the characteristics of regions of strong intraseasonal and interannual variability (low SCR) versus highly seasonal regions (high SCR).

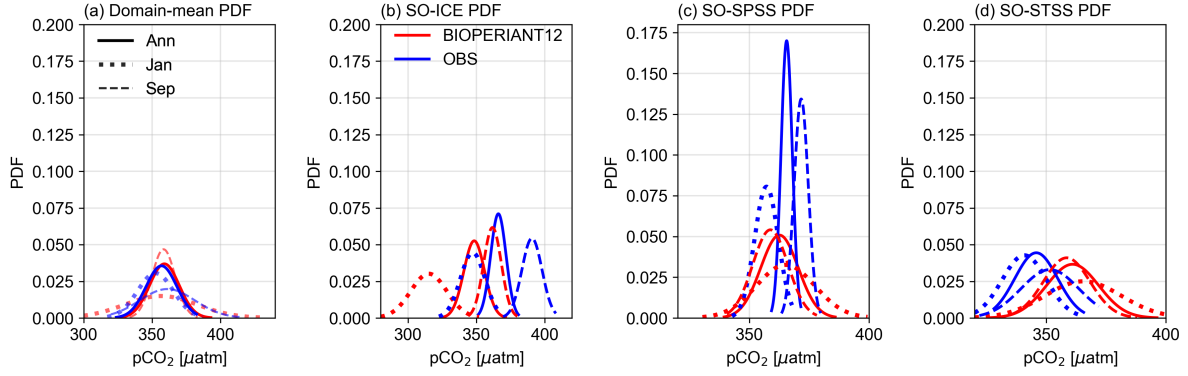

Figure S13. BIOPERIANT12 (red) versus CSIR-ML6 (blue) pCO_2 seasonal PDF comparison for **(a)** model domain, **(b)** SO-ICE, **(c)** SO-SPSS, and **(d)** SO-STSS biomes. Showing annual (solid line), January (dotted line), and September (dashed line) monthly climatologies.

S4.1 Carbon seasonal cycles differences

The model's poor skill in representing the seasonal cycle of pCO_2 and FCO_2 in the SO-SPSS and SO-STSS relative to the CSIR-ML6 dataset may be due to weaker seasonal vertical dissolved inorganic carbon (DIC) fluxes. While the model overestimates the mean state DIC magnitudes with respect to observed estimates (Fig 7e, Fig.S14), it underestimates the upper ocean DIC gradients (Fig. S11). This leads to a weaker DIC entertainment potential during the seasons of enhanced vertical mixing, and hence a diminished seasonal DIC variability (Mongwe et al., 2016). Further, the model's exaggeration of total alkalinity (TA) and DIC mean states (Fig. 7, S11) leads to a high Revelle factor and hence a greater ocean pCO_2 sensitivity to temperature seasonal changes (Vaittinada Ayar et al., 2022; Rodgers et al., 2023). The greater sensitivity of ocean pCO_2 to temperature changes with respect to observed estimates may therefore explain the model's tendency to be dominated by the thermal pCO_2 component in the SO-SPSS and SO-STSS, which disagrees with observed estimates. The exception of the dominant role of the non-thermal pCO_2 in the SO-ICE is likely due to the exaggeration of the biological processes on the surface DIC, shown by the overstimulation of chlorophyll (Fig 7i).

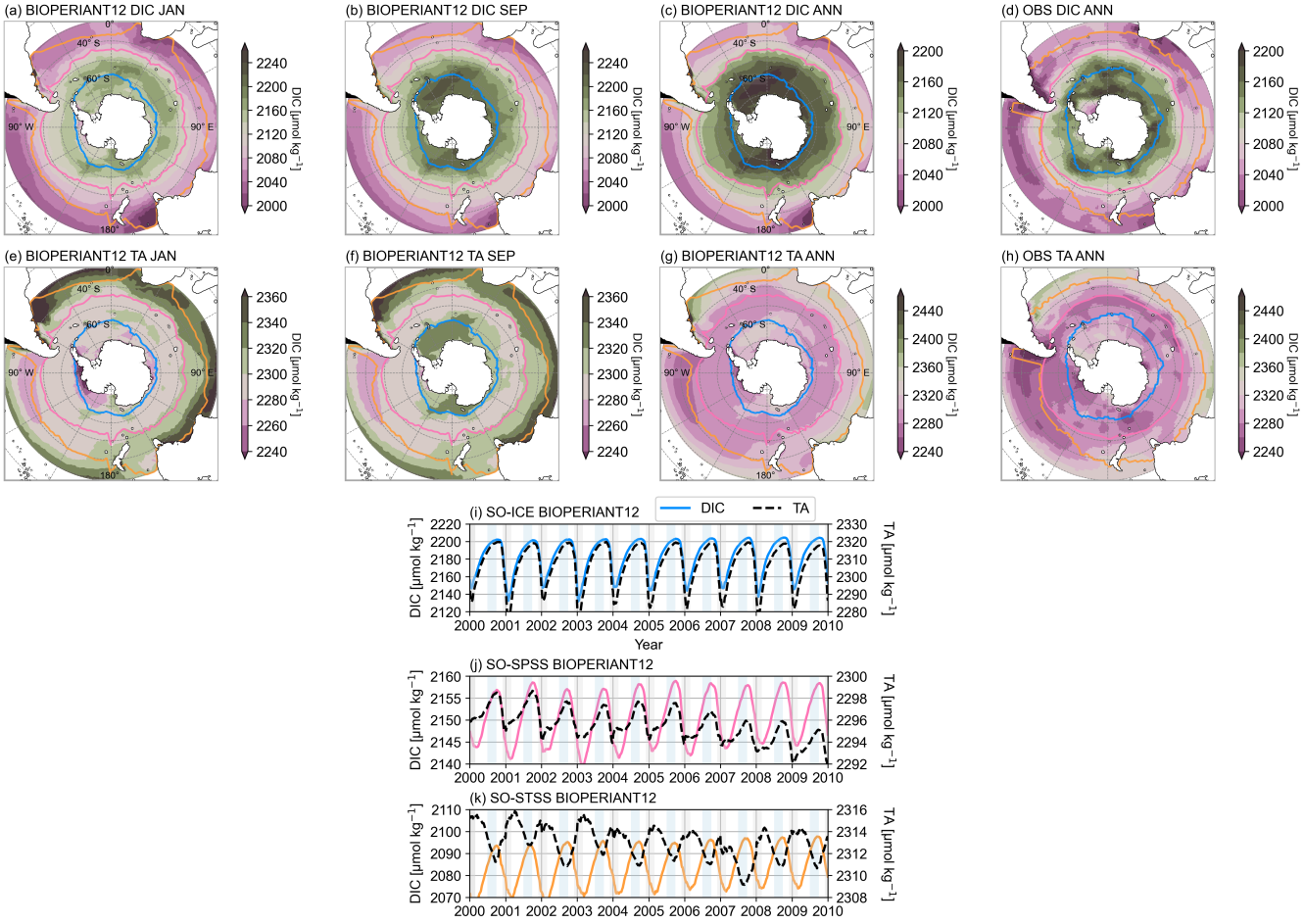

Figure S14. Climatological mean surface maps for DIC for BIOPERIANT12 **(a)** January , **(b)** September OBS Glodap v2, **(c)** annual mean, compared against **(d)** GLODAP v2 DIC annual mean; and Total Alkalinity (TA) for BIOPERIANT12 **(e)** January, **(f)** September, **(g)** annual mean; against **(h)** Glodap v2 TA annual mean. Model-only evolution of area-weighted, domain-averaged DIC and TA for biomes **(i)** SO-ICE, **(j)** SO-SPSS, and **(k)** SO-STSS.

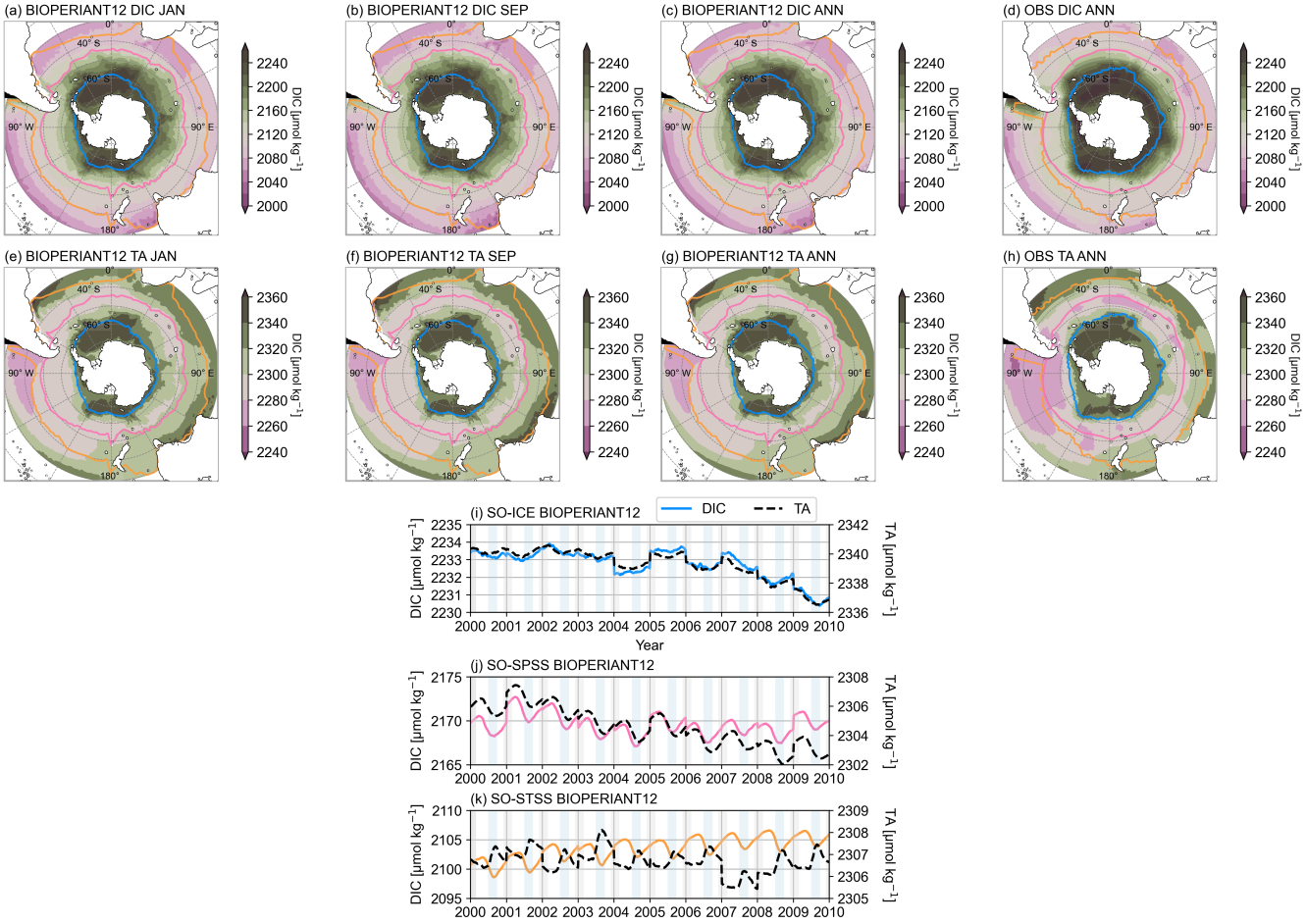

Figure S15. Climatological mean maps for DIC and TA as above for 200 m depth.

S5 Nutrients

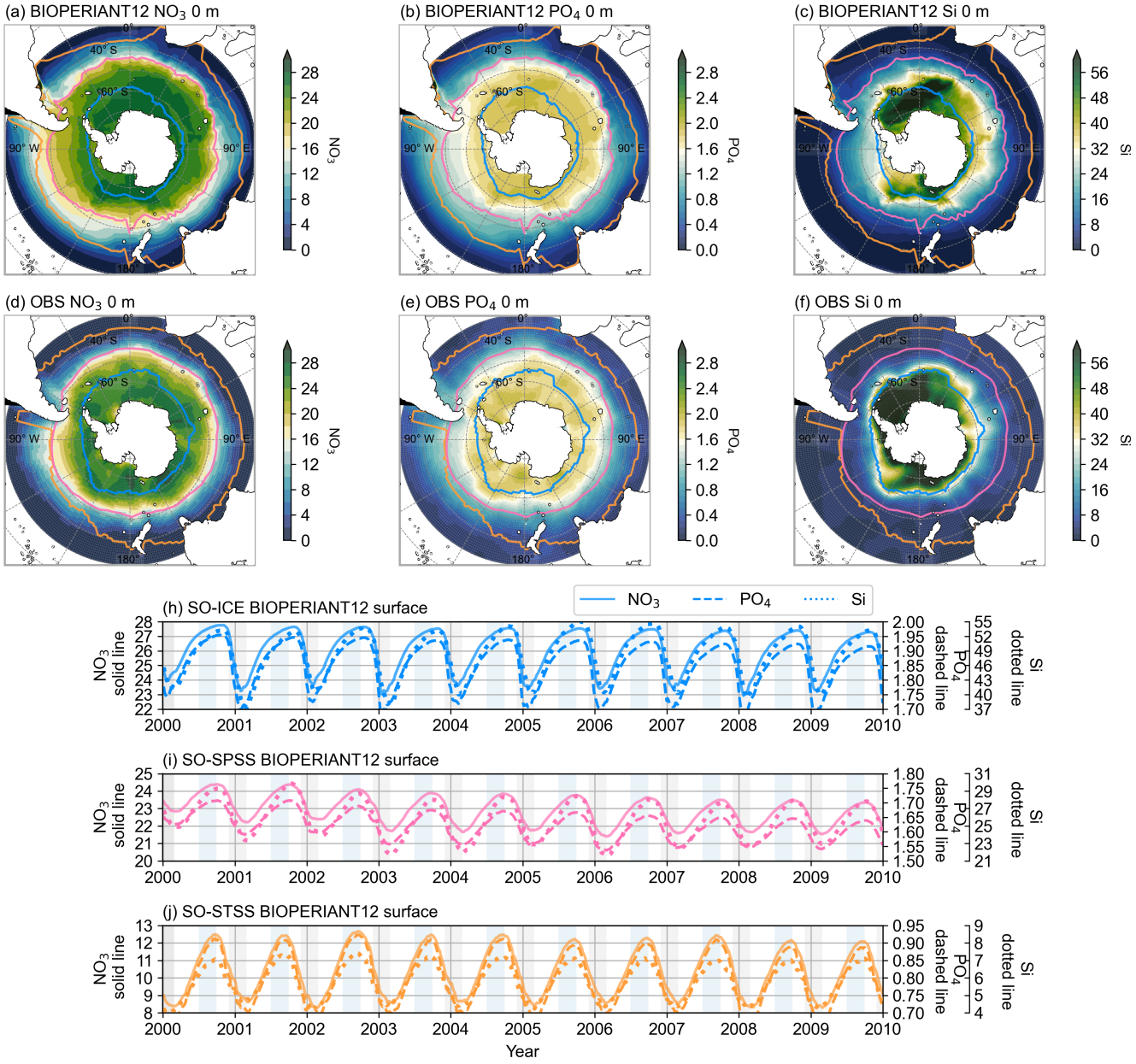

Figure S16. BIOPERIANT12 versus WOA climatological mean surface concentrations for **(a, d)** nitrate, **(b, e)** phosphate, and **(c, f)** silicate, respectively. Model only evolution of same variables over **(h)** SO-ICE, **(i)** SO-SPSS, and **(j)** SO-STSS biomes.

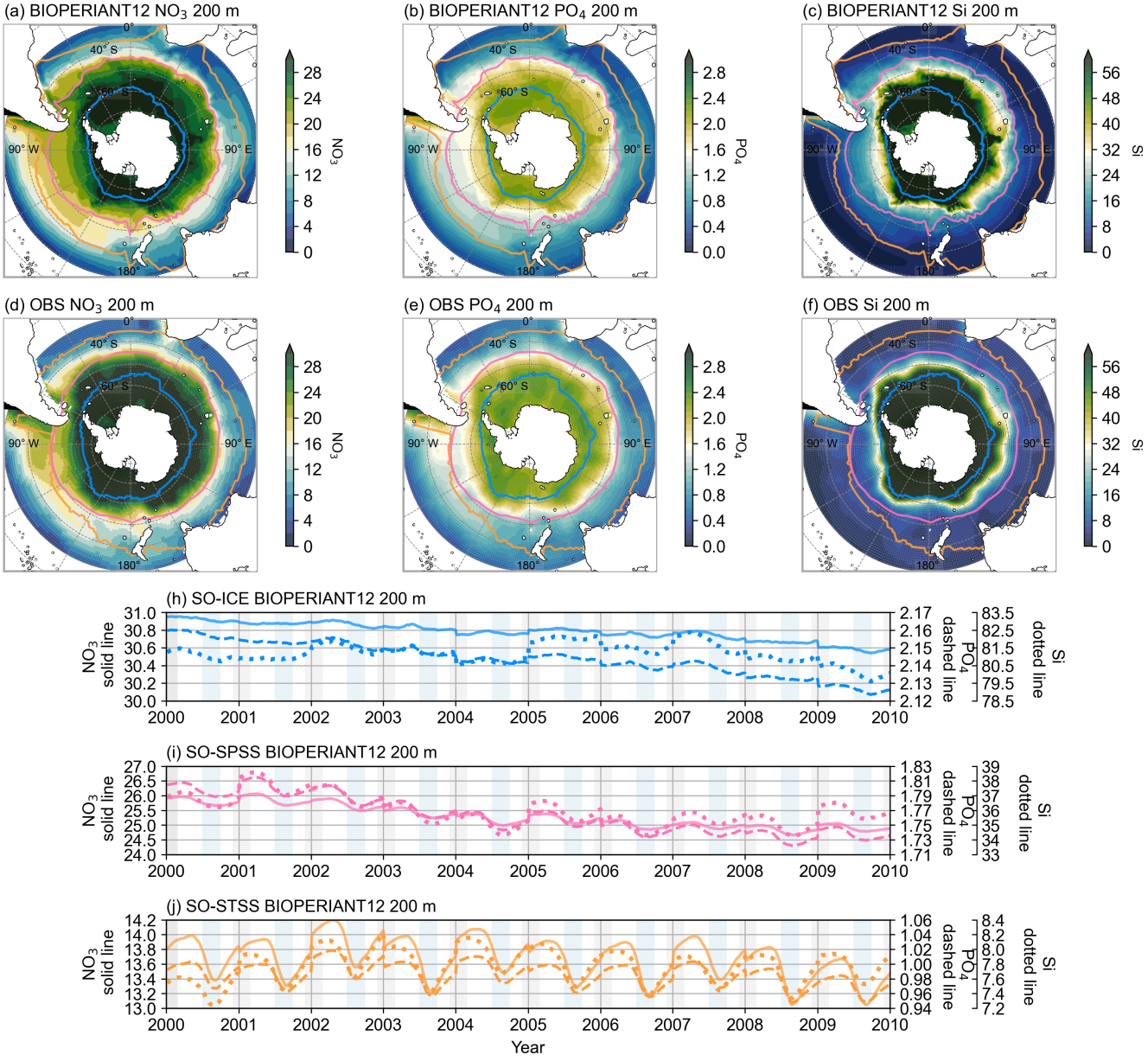

Figure S17. BIOPERIANT12 versus WOA climatological mean 200 m concentrations for **(a, d)** nitrate, **(b, e)** phosphate, and **(c, f)** silicate, respectively. Model only evolution of same variables over **(h)** SO-ICE, **(i)** SO-SPSS, and **(j)** SO-STSS biomes.

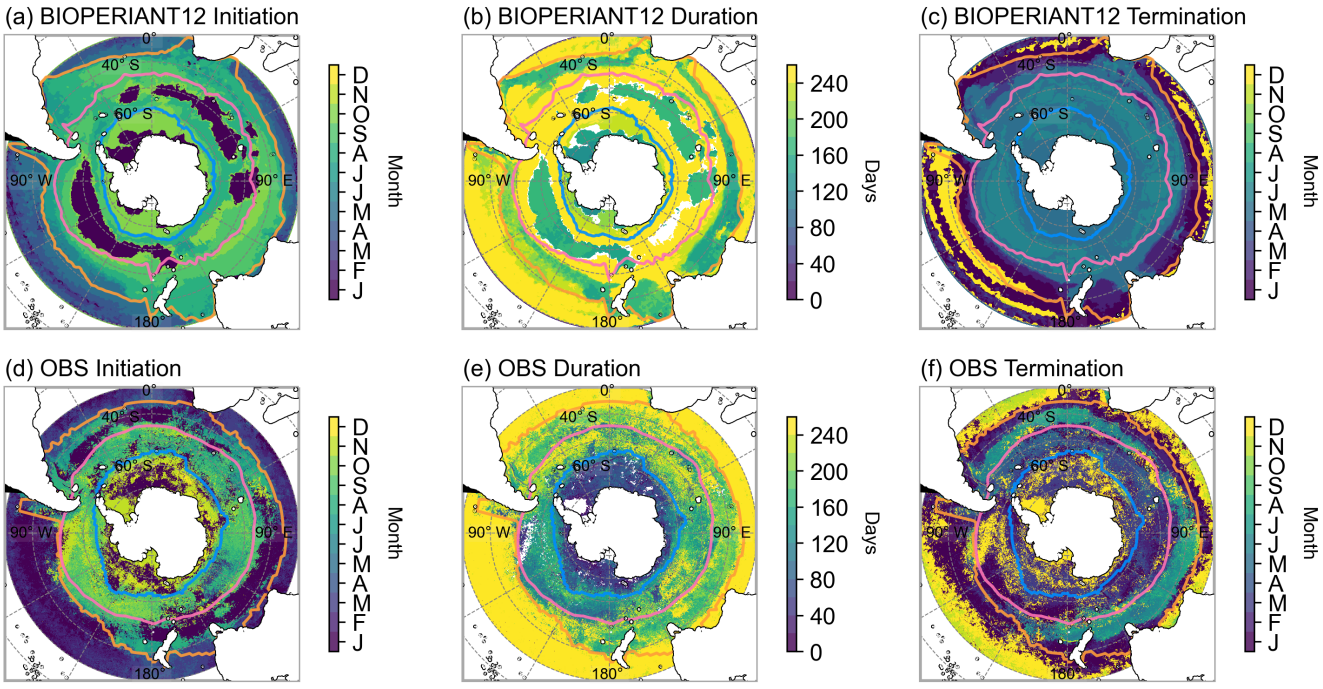

Figure S18. Regional distribution of chlorophyll initiation, duration and termination dates for **(a, b, c)** BIOPERIANT12 and **(d, e, f)** OCCCI v6 data..

References

Fay, A. R. and McKinley, G. A.: Global Open-Ocean Biomes: Mean and Temporal Variability, Earth System Science Data, 6, 273–284, https://doi.org/10.5194/essd-6-273-2014, 2014.

Freeman, N. M. and Lovenduski, N. S.: Mapping the Antarctic Polar Front: weekly realizations from 2002 to 2014, Earth System Science Data, 8, 191–198, https://doi.org/10.5194/essd-8-191-2016, 2016.

Mongwe, N. P., Chang, N., and Monteiro, P. M. S.: The Seasonal Cycle as a Mode to Diagnose Biases in Modelled CO2 Fluxes in the Southern Ocean, Ocean Modelling, 106, 90–103, https://doi.org/10.1016/j.ocemod.2016.09.006, 2016.

Orsi, A. H., Whitworth, T., and Nowlin, W. D.: On the Meridional Extent and Fronts of the Antarctic Circumpolar Current, Deep Sea Research Part I: Oceanographic Research Papers, 42, 641–673, https://doi.org/10.1016/0967-0637(95)00021-W, 1995.

Rodgers, K. B., Schwinger, J., Fassbender, A. J., Landschützer, P., Yamaguchi, R., Frenzel, H., Stein, K., Müller, J. D., Goris, N., Sharma, S., et al.: Seasonal variability of the surface ocean carbon cycle: A synthesis, Global Biogeochemical Cycles, 37, e2023GB007 798, 2023.

Vaittinada Ayar, P., Bopp, L., Christian, J. R., Ilyina, T., Krasting, J. P., Séférian, R., Tsujino, H., Watanabe, M., Yool, A., and Tjiputra, J.: Contrasting projections of the ENSO-driven CO_2 flux variability in the equatorial Pacific under high-warming scenario, Earth System Dynamics, 13, 1097–1118, https://doi.org/10.5194/esd-13-1097-2022, publisher: Copernicus GmbH, 2022.